remote sensing

MDPI

Article

Mapping Kinetic Energy Hotspots in the Persian Gulf and Oman Sea Using Surface Current Derived by Geodetic Observations and Data Assimilation

Mahmoud Pirooznia [1], Behzad Voosoghi [1], Mohammad Amin Khalili [2,*], Diego Di Martire [2] and Arash Amini [1]

[1] Faculty of Geodesy and Geomatics Engineering, K. N. Toosi University of Technology, Tehran 15433-19967, Iran; ma.pirooznia@email.kntu.ac.ir (M.P.); vosoghi@kntu.ac.ir (B.V.); a_amini@email.kntu.ac.ir (A.A.)
[2] Department of Earth Sciences, Environment, and Resources, University of Naples, Federico II, 80126 Naples, Italy; diego.dimartire@unina.it
* Correspondence: mohammadamin.khalili@unina.it; Tel.: +39-3444137462

Abstract: Harnessing ocean kinetic energy has emerged as a promising renewable energy solution in recent years. However, identifying optimal locations for extracting this energy remains a significant challenge. This study presents a novel scheme to estimate the total surface current (TSC) as permanent surface current by integrating geodetic data and in-situ measurements. The TSC is typically a combination of the geostrophic current, derived from dynamic topography, and the Ekman current. We utilize NOAA's Ekman current data to complement the geostrophic current and obtain the TSC. To further enhance the accuracy of the TSC estimates, we employ a 3DVAR data assimilation method, incorporating local current meter observations. The results are verified against two control current meter stations. The data-assimilation process resulted in an improvement of 4 to 15 cm/s in the precision of calculated TSC. Using the assimilated TSC data, we then assess the kinetic energy potential and identify six regions with the most significant promise for marine kinetic energy extraction. This innovative approach can assist researchers and policymakers in targeting the most suitable locations for harnessing renewable ocean energy.

Keywords: data assimilation; geodetic data; geostrophic current; Ekman current; surface current; kinetic energy

Citation: Pirooznia, M.; Voosoghi, B.; Khalili, M.A.; Di Martire, D.; Amini, A. Mapping Kinetic Energy Hotspots in the Persian Gulf and Oman Sea Using Surface Current Derived by Geodetic Observations and Data Assimilation. *Remote Sens.* **2024**, *16*, 3340. https://doi.org/10.3390/rs16173340

Academic Editors: Daniele Ciani and Milena Menna

Received: 20 July 2024
Revised: 4 September 2024
Accepted: 6 September 2024
Published: 9 September 2024

1. Introduction

The potential of ocean kinetic energy as a renewable resource has been widely recognized in recent years. Numerous studies have highlighted the significant energy-generating capacity of the world's oceans [1]. However, successfully harnessing this energy presents a considerable challenge, as identifying optimal locations for extraction remains complex [2]. The search for renewable and sustainable energy sources has become increasingly urgent as the world grapples with climate change and fossil fuel depletion [3,4]. In this context, harnessing ocean kinetic energy has emerged as a promising solution [5]. Ocean currents, tides, and waves possess significant kinetic energy that can be converted into electricity through technologies like tidal turbines, wave energy converters, and ocean current turbines [6,7]. Among the ocean energy resources, extracting kinetic energy from ocean surface currents offers advantages such as a more consistent and predictable energy supply, reduced environmental impact, and potential integration with existing infrastructure [8,9]. Studies estimate the global technical potential for ocean current energy extraction could reach 5000 Terawatt-hours (TWh) per year, making it a largely untapped renewable resource [2].

Ocean surface currents are driven by various factors, including wind, tidal forces, and density gradients [6]. Multiple methods are used to calculate and understand ocean currents, including in situ direct measurements from moored and drifting current meters,

vessel-mounted acoustic doppler current profilers (ADCPs), equipment was sourced from reputable manufacturers such as Teledyne Marine (USA), Nortek (Norway), RDI (USA), Kongsberg Maritime (Norway), SonTek (USA), Aanderaa Data Instruments (Norway), and Sea-Bird Scientific (USA), and numerical ocean models that simulate the complex physical processes driving global ocean circulation [8,9]. Additionally, satellite altimetry and geodetic data can be combined to derive detailed estimates of ocean dynamic topography, which can then be used to calculate surface current speed and direction [10–13]. However, successfully deploying ocean current energy extraction technologies requires a comprehensive understanding of surface currents' spatial and temporal distribution and the identification of optimal locations, which has been challenging due to ocean processes' complex and dynamic nature [2,10]. To address this, integrating satellite altimetry and geodetic data has enabled more detailed mapping and analysis of global ocean surface currents, potentially revolutionizing our understanding and informing applications ranging from marine spatial planning to optimizing ocean renewable energy extraction [14,15]. Yet, capturing the full spatio-temporal complexity of the ocean surface current field remains a challenge, as satellite-derived estimates may not always capture the critical small-scale features and high-frequency variability [16,17]. Direct measurements can provide valuable information on the fine-scale structure and temporal evolution of surface currents often missed by satellite observations [18]. By assimilating these in situ data sources into ocean circulation derived by satellite altimetry and numerical models, scientists can create more comprehensive and accurate representations of the ocean current system, better capturing the complex interplay of physical processes that drive global ocean circulation [15,19]. This improved understanding of the ocean surface current field can support more efficient maritime operations, better predict the spread of pollutants, and optimize the placement and operation of marine renewable energy devices [20]. Additionally, more accurate surface current data can significantly advance climate modeling, oceanographic research, and our overall understanding of the global ocean system [21–23].

The Persian Gulf and Oman Sea are the geographic regions examined in this study, regions known for their strategic importance, diverse marine environments, and the need for enhanced ocean current data to address various environmental and economic challenges [13–15]. In this study, a data-driven scheme is presented to improve the total surface current (TSC) as permanent surface current in the Persian Gulf and Oman Sea. In the proposed method, the dynamic topography obtained by geodetic data sources, described in our previous study [13], is used to calculate the monthly geostrophic current from 2002 to 2022. Then, the TSC is determined; this is done by summing the geostrophic current and Ekman current. In addition, the estimated TSC is improved by integrating local current meter observations using the 3DVAR data assimilation technique within the study region. Finally, the kinetic energy potential is assessed using the assimilated TSC data, and then the most appropriate locations for harnessing the kinetic energy are selected. The workflow for this study is illustrated in Figure 1. It is important to note that tidal energy is a highly significant and promising source of marine renewable energy. However, this study aims to identify locations suitable for utilizing the kinetic energy from the permanent surface currents in the study area.

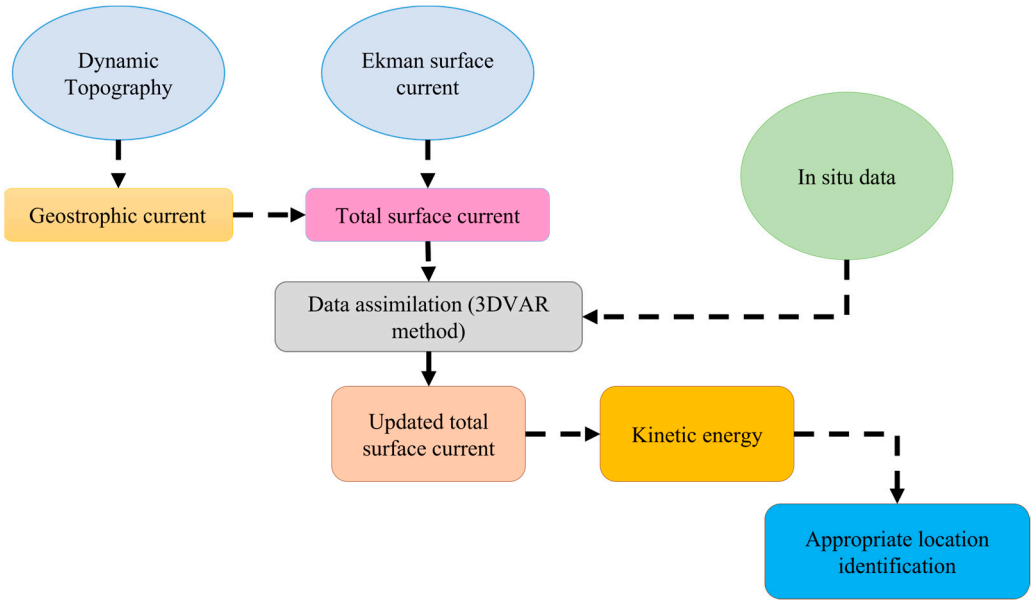

Figure 1. The flowchart of the proposed scheme.

2. Materials and Methods

2.1. Data Description

The dataset used in this study consists of the dynamic topography derived by utilizing geodetic data sources in our previous study [13]. The dynamic topography was evaluated using the variance component estimation (VCE) method by combining two data sources: (i) satellite altimetry data to directly observe sea surface height, with all necessary corrections, such as retracking, ionospheric, and other relevant adjustments, having been applied to the altimetry observations in both offshore and nearshore regions [24,25]; and (ii) hydrographic (salinity and temperature) and Gravity Recovery and Climate Experiment (GRACE) data, which were used to compute the steric (due to changes in water density) and non-steric (due to mass changes) components of sea level anomalies.

The previous study [13] utilized the VCE approach to provide more accurate and reliable dynamic topography estimates, particularly in coastal regions where altimetry data alone may be insufficient due to the challenges of altimetry in those areas [13,24,25]. A key advantage of this integrated approach is the adaptive weighting strategy used in the VCE process. By assigning suitable initial weights to the altimetry and hydrographic + GRACE data, the method can leverage the strengths of each data source and compensate for their respective limitations. In nearshore areas, where altimetry observations are known to be less accurate, the hydrographic + GRACE data are given greater weight to enhance the reliability of the dynamic topography estimation. Conversely, in offshore regions where altimetry performs well, more emphasis is placed on the altimetry data. This issue is important because it is crucial to have an optimal dynamic topography and its covariance matrix to form the background or model covariance matrix in the data-assimilation process. The resulting dynamic topography data were provided from 2002 to 2022 at a monthly temporal interval and a spatial resolution of 0.25 degrees as described [13]. These data calculate the geostrophic component of the total ocean surface current field.

Moreover, the Ekman surface current data provided by the National Oceanic and Atmospheric Administration (NOAA) have a monthly temporal resolution and 0.25 degrees spatial resolution from 2002 to 2022, and are available at the following URL: "https://coastwatch.pfeg.noaa.gov/erddap/info/erdlasFnWPr/index.html (accessed on 5 September 2024)". Ekman surface currents refer to the circular movement of water in the upper ocean layer caused by the interaction between wind stress and the Coriolis effect [21]. NOAA gathers Ekman surface current data from various sources, including: (i) satellite-based measurements of ocean surface winds and currents, (ii) in situ measurements from

moored and drifting buoys, and (iii) numerical ocean circulation models that incorporate wind and other forcing data [21]. NOAA's estimates of Ekman surface currents are based on the classic Ekman theory, which describes the spiral-shaped movement of surface currents driven by wind stress and the Coriolis effect. NOAA first calculates the Ekman transport, the net movement of water in the Ekman layer, from the wind stress data and then uses this to derive the Ekman surface current [21]. However, Ekman's current estimates have several limitations and potential uncertainties. The underlying data sources, such as the satellite wind data or the ocean model grid, may limit the spatial and temporal resolution of the estimates. The assumption of a constant Ekman layer depth may not always be accurate, as the depth can vary due to factors like stratification, upwelling, and other physical processes. The Ekman current estimates may also have biases or random errors due to the challenges in validating the data against in situ measurements, which can be sparse or unevenly distributed. Additionally, the numerical ocean models used to simulate Ekman dynamics have their own set of limitations and simplifications, which can introduce uncertainties in the final Ekman current estimates. Furthermore, factors like coastal topography, eddies, and other local effects may not fully capture the large-scale Ekman current estimates, leading to discrepancies in specific regions [21].

These Ekman current estimates are combined with the geostrophic currents to compute the TSC field. The dynamic topography and Ekman surface current grid data are interpolated onto a 0.1-degree resolution grid using the Kriging interpolation method to generate TSC [13]. This interpolation process may introduce errors, another data preparation limitation.

To overcome the limitations and potential uncertainties mentioned in the data and enhance the accuracy of estimated TSC, the data assimilation process on the product obtained from these data is done using local current measurements sourced from multiple monitoring stations. The details of these current measurement sites are provided in Table 1 and Figure 2. The data from these locations are obtained from the Ports and Maritime Organization (PMO) of Iran. It is important to note that the Nakhl Taghi and Konarak stations are not used for the data assimilation process itself but rather serve as independent validation points to assess the performance of the assimilated TSC estimates.

Table 1. Current meter stations features.

ID	Geographic Region	Instrumentation	Coordinates (Lat, Lon)	Periods (mm-dd-yyyy)	Sources
1	Khuran	ADCP	28.01, 55.45	08-30-2005 to 10-04-2005	INIO
2	Konarak	ADCP	25.37, 60.43	08-21-2006 to 09-03-2007	PMO
3	Chabahar	ADCP	25.29, 60.67	08-21-2006 to 09-03-2008	PMO
4	Bushehr	ADCP	28.97, 50.66	06-15-2010 to 07-26-2011	PMO
5	Taheri	ADCP	27.63, 52.36	08-23-2018 to 09-24-2022	PMO
6	Nayband Gulf	ADCP	27.42, 52.65	05-11-2009 to 07-12-2009	PMO
7	Nakhl Taghi	ADCP	27.49, 52.57	08-22-2008 to 09-24-2009	PMO
8	Kangan	ADCP	26.83, 52.04	08-23-2008 to 09-25-2009	PMO
10	Jask	ADCP	26.05, 57.76	07-16-2010 to 01-23-2011	PMO
11	Hormuz	ADCP	27.15, 56.46	10-06-2009 to 10-12-2010	PMO
12	Googsar	ADCP	25.78, 57.77	07-12-2010 to 10-28-2010	PMO
13	Rajaei	ADCP	27.07, 56.08	10-12-2009 to 01-12-2010	PMO

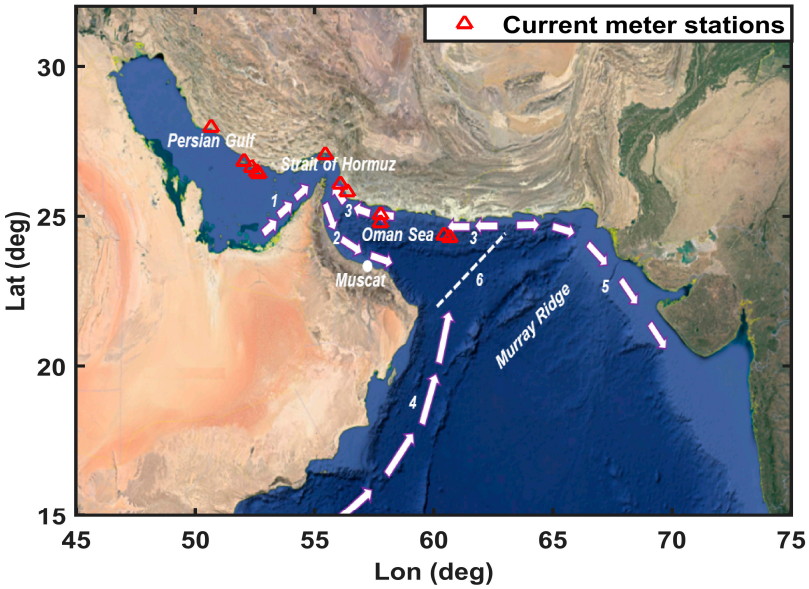

Figure 2. Study area and current meter stations. Background image from "www.earth.google.com (accessed on 5 September 2024)" (1) and (2): the outward flow from the Persian Gulf into the Gulf of Oman, (3): inflow of the Oman Sea to the Persian Gulf, (4): Oman coastal current, (5): Indian coastal current, and (6): dashed line indicating the location of the Ras Al-Hadd region.

Another independent dataset for validating the assimilated TSC is the surface current product from the Copernicus marine environment monitoring service (CMEMS), which is available on the website "https://data.marine.copernicus.eu/product/GLOBAL_MULTIYEAR_PHY_001_030/description (accessed on 5 September 2024)"; the data show a monthly temporal resolution and a spatial resolution of 0.083 degrees from 2002 to 2024 on 50 standard vertical levels, and the surface layer (Level 1) data are used for validation procedure. This ocean model is based on the Nucleus for European Modelling of the Ocean (NEMO) numerical model, version 3.1, which assimilates in situ and satellite data, such as altimetry measurements, to represent the ocean state comprehensively. Detailed information about the CMEMS model, including computational aspects, error characteristics, and biases, is available in the quality information document at "https://catalogue.marine.copernicus.eu/documents/QUID/CMEMS-GLO-QUID-001-030.pdf (accessed on 5 September 2024)".

Rigorous data quality assurance and control processes have been implemented for all the information utilized in this study. These measures include the identification and removal of erroneous observations, as well as comprehensive outlier detection and mitigation. For a detailed description of the specific quality control techniques employed, please refer to the methodology outlined in our previous publication [13,15].

2.2. Methodology

In this section, the mathematical description of the methodology of the proposed approach for extracting kinetic energy from the Sea is described according to the flowchart of Figure 1. First, the dynamic topography is used to calculate the geostrophic current. Then, the Ekman surface current represents the wind-driven surface current, combined with the geostrophic current to obtain the TSC. Next, the data assimilation step uses the 3DVAR (3-Dimensional Variational) method to integrate the in situ current observations with the TSC calculated from the geostrophic and Ekman currents, which helps to improve the accuracy of the TSC estimates. The data-assimilation process results in an updated, more accurate TSC. The in situ current meter observations are used in the data-assimilation step to enhance the TSC estimates. The updated, assimilated TSC is then used to calculate the kinetic energy potential, which can help identify the most promising marine kinetic energy extraction

locations. The final step is to use the kinetic energy estimates to determine the appropriate location identification for harnessing renewable ocean energy in the study region.

2.2.1. Estimation of TSC

The total ocean surface current field is estimated by combining two key components:

(i) The Ekman surface current is obtained from data provided by the NOAA.

(ii) The geostrophic current is computed by determining the zonal (u) and meridional (v) velocity components based on the horizontal gradient of the dynamic topography (DT), as detailed in our previous studies [13,14]. The specific equations used to compute the geostrophic velocity components are provided below [13,14]:

$$\begin{aligned} u &= -\frac{g}{f}\frac{\partial \zeta}{\partial y} \\ v &= \frac{g}{f}\frac{\partial \zeta}{\partial x} \end{aligned} \tag{1}$$

where g is the acceleration due to gravity, ζ represents the dynamic topography, which is a key input variable; $f = 2\Omega\sin\phi$ is the Coriolis parameter, with Ω being the angular velocity of the Earth's rotation and ϕ denoting the latitude. Finally, the total ocean surface current can be estimated by summing the Ekman current component obtained from NOAA data and the geostrophic current components computed from the dynamic topography gradients, as shown by the following equation [14]:

$$\begin{aligned} &u_{Total} = u_{Geostrophic} + u_{Ekman}, \;\; v_{Total} = v_{Geostrophic} + v_{Ekman} \\ &W_{Total} = \sqrt{{u_{Total}}^2 + {v_{Total}}^2} \end{aligned} \tag{2}$$

This combined approach allows us to capture the full complexity of the study region's total ocean surface current field.

2.2.2. Assimilation Using the 3DVAR Method

The 3DVAR data-assimilation process involves minimizing an objective function that balances the differences between the model state (estimated TSC using Equations (1) and (2)) and the observations (local current meter data) while accounting for the uncertainties, including both random errors and potential biases, in both the model and the observations. To improve the results obtained from the TSC estimates, the 3DVAR method uses data assimilation with the following objective function [26–28].

$$J(x) = \frac{1}{2}(x - x^b)^T B^{-1}(x - x^b) + \frac{1}{2}(y - Hx^b)^T R^{-1}(y - Hx^b) \tag{3}$$

where x is the state vector to be optimized (assimilated TSC), x^b is the model or referenced state vector (estimated TSC), B is the error covariance matrix associated with the reference state (variance-covariance matrix of estimated TSC), H is the observation that relates the state vector to the observation space, y is the observation vector (in situ data), and R represents the error covariance matrix associated with the observations. The goal is to find the optimal state vector x that minimizes this objective function, incorporating both the background information (the model state) and the observational data through the 3DVAR data assimilation approach. In the above equation, the minimized solution of the objective function is obtained by the calculation $\nabla J(x) = 0$. By setting the gradient $\nabla J(x)$ equal to zero and solving for x, the minimized solution that best fits both the background information and the observational data can be obtained through the 3DVAR data-assimilation approach [28].

$$\begin{aligned} x &= x^b + W(y - Hx^b) \\ W &= BH^T(HBH^T + R)^{-1} \end{aligned} \tag{4}$$

Here, W is called the gain matrix. The matrix B can be formulated using the equation below [14].

$$B = \mathrm{cov}\begin{pmatrix} u_{Total} \\ v_{Total} \end{pmatrix} = \left[\frac{g^2}{f^2} \mathrm{cov}\begin{pmatrix} \partial\zeta/\partial y \\ \partial\zeta/\partial x \end{pmatrix} + \mathrm{cov}\begin{pmatrix} u_{Ekman} \\ v_{Ekman} \end{pmatrix} \right] \quad (5)$$

One point that should be noticed is that the covariance matrix of the dynamic topography is derived from the referenced study [13], and the identity matrix represents the covariance of the Ekman current components.

Alongside the limitations in the data mentioned in Section 2.1, the approximations made in the geostrophic current equation (Equation (1)) introduce uncertainties in estimating the TSC. This simplification and approximation include the assumption of hydrostatic balance. This assumption means that the weight of the water column balances the vertical pressure gradient. This allows the pressure to be expressed in terms of the density and the height of the water column. Additionally, computational errors in solving equations, such as rounding errors, can cause the results to deviate from the actual values [29]. The data-assimilation procedure may help reduce biases in the model. By carefully constructing the covariance matrices for observations (R) and the model (B), increasing the weight given to the unbiased observations (y) can help mitigate the bias in the model to a certain extent. The key is to provide more weight to local observations that are trusted to be unbiased. This reduces the influence of the model's biases on the final estimate. This is achieved by applying an appropriate variance factor to the observations, effectively downweighing the model's biased components. In other words, by adjusting the variance factors for both the observations and the model, the overall uncertainties in the estimate can be mitigated to a certain extent through the data-assimilation process. The main point is that carefully accounting for and balancing the relative weights of unbiased observations and the model can help compensate for the uncertainties in the model, leading to improved estimates. Moreover, to quantify the impact of the data assimilation, the model estimates (estimated TSC) before assimilation as x^b and the estimates after assimilation as x can be compared with in situ current meter data in control stations. Therefore, two control stations are provided for this purpose.

2.2.3. Estimation of Kinetic Energy

Researchers worldwide have focused on using marine renewable energies utilizing ocean currents in recent decades. Given Iran's extensive coastal region, both persistent and transient current patterns exist, exhibiting varied speeds and orientations in the country's water borders. Ocean renewable energy technologies include the utilization of kinetic energy created by seawater currents. This is achieved by identifying the areas where kinetic energy is significant and installing equipment with different turbines to generate electricity. In the past, the equipment designed in this field could generate 100 watts of electrical power at a flow speed of 1.2 m per second, but today, this capability is possible with a current speed of 60 to 80 cm per second. This technology currently exists in developed countries. Therefore, we are looking to identify the areas with potential kinetic energy in the Persian Gulf and the Oman Sea. To this end, we will calculate the kinetic energy content of the ocean current within the study area using the following equation [30].

$$\begin{aligned} \overline{u} &= \frac{1}{N}\sum_{k=1}^{N} u_{Total}^{k}, \quad \overline{v} = \frac{1}{N}\sum_{k=1}^{N} v_{Total}^{k} \\ E &= \frac{\overline{u}_{Total}{}^2 + \overline{v}_{Total}{}^2}{2} \end{aligned} \quad (6)$$

where $\overline{u}$ and $\overline{v}$ represent the average components of the TSC in the east-to-west and north-to-south directions, respectively, and E represents the kinetic energy derived from the ocean current.

3. Results

The focus of this section is on presenting and analyzing the results. Generally, three steps according to methodology are applied: (i) the estimation of TSC, (ii) the data-assimilation procedure for improvement of TSC, and (iii) the estimation of kinetic energy.

As mentioned before, the TSC is calculated by computation of geostrophic and Ekman current components. The geostrophic current is computed using the dynamic topography derived from our previous study [13] via geodetic data sources. Additionally, the Ekman current data from NOAA are utilized in evaluating the TSC.

Figure 2 shows the direction of the geostrophic currents in the Persian Gulf, the Oman Sea, and the northern Indian Ocean, estimated from the mean of the total monthly currents from 2002 to 2022. The analysis of monthly geostrophic currents from 2002 to 2022 reveals the following patterns. (i) In the Persian Gulf region bounded by 47 to 55 degrees east longitude and 24 to 30 degrees north latitude, the monthly geostrophic currents exhibit a relatively consistent behavior, including the inflow from the Gulf of Oman, the outflow to the Gulf of Oman, and the presence of a coastal current. (ii) Conversely, in the Gulf of Oman region spanning 57 to 58 degrees east longitude and 24 to 25 degrees north latitude, the current patterns show more variability across different months, potentially influenced by seasonal changes and water exchange between the Persian Gulf and the Gulf of Oman. (iii) Further south, in the region encompassing 65 to 70 degrees east and 22 to 26 degrees north, the geostrophic current maintains a consistent eastward direction along the southern coasts of India. (iv) Regarding the Arabian Sea region near the Oman coast, spanning 52 to 57 degrees east and 16 to 22 degrees north, the current pattern exhibits some variability across different months. However, the overall trend indicates that the coastal current in this area flows towards the northern Indian Ocean.

Notably, the Ekman current taken from NOAA also shows monthly variations. The Ekman current can amplify some of the physical phenomena of the water, such as upwelling and downwelling, which can consequently lead to specific impacts on the environment, fishing, and small-scale fisheries [31]. The direction of the Ekman surface currents in the Persian Gulf and Oman Sea regions is different everywhere and utterly dependent on the direction of the wind. This direction is seaward when the westerly winds blow, resulting in upwelling currents, and shoreward when the easterly winds blow, creating downwelling currents. Focusing on the northern Persian Gulf and the northwestern Oman Sea region, the Ekman current induces upwelling currents, bringing the cold subsurface waters to the sea surface. This phenomenon leads to changes in the surface water temperature and the displacement of nutrients in the water. As a result, the food web is enhanced, and consequently, the population of marine organisms, especially fish, increases [31]. This highlights the importance of the Ekman current and the effects of wind on ocean circulation. Finally, the TSC is calculated by combining the geostrophic and Ekman surface currents. Illustrated in Figure 3 is a representative example of the components of the mean TSC in January (this figure is the monthly average of the TSC for all of January from 2002 to 2022).

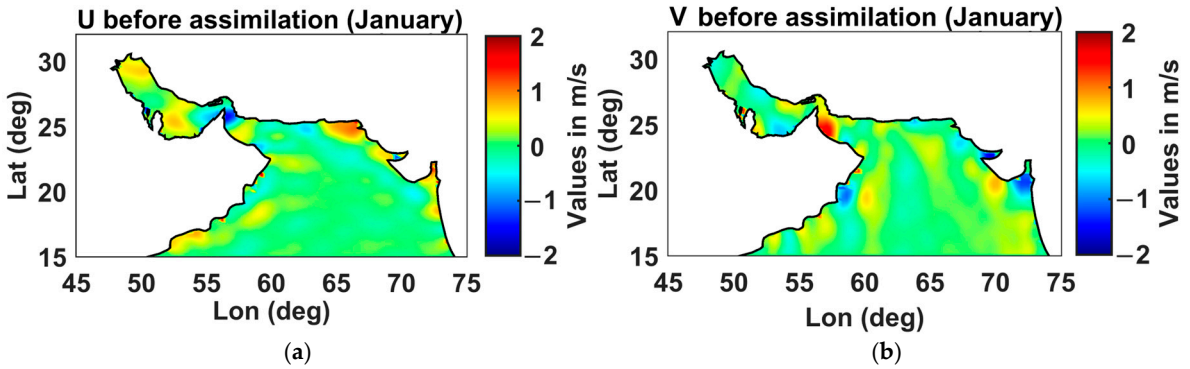

Figure 3. The components of the TSC (U and V) in January. U (**a**) and V (**b**).

As a typical example, the pattern of TSCs for the month of January is shown in Figure 4. For further investigation, the study area is divided into three regions: the Oman Sea (region 1), the Persian Gulf (region 2), and the Strait of Hormuz (region 3), and the statistical parameters of the current velocity in these areas are examined. Table 2 shows the statistical characteristics of the current velocity in different months between 2002 and 2022 for the three mentioned regions. The maximum marine current velocity in the Oman Sea, the Persian Gulf, and the Strait of Hormuz is approximately 110 cm/s in April, around 134 cm/s in November, and about 135 cm/s in December, respectively. Given the strategic importance of the Strait of Hormuz, a few grid points within the strait are considered for analysis from 2002 to 2022. At these points, the maximum current speed is 135 cm/s, and the minimum is 103 cm/s between 2002 and 2022. Also, the average current speed is approximately 125 cm/s. One point that should be noticed is that this region has significant tidal potential, which is highly important for exploiting marine energy. However, this study aims to investigate the permanent surface currents and identify the kinetic energy that can be harnessed from them; geostrophic and Ekman currents do not solely drive the flow through the Strait of Hormuz but are also influenced by other factors such as tides, instantaneous winds, etc. [32].

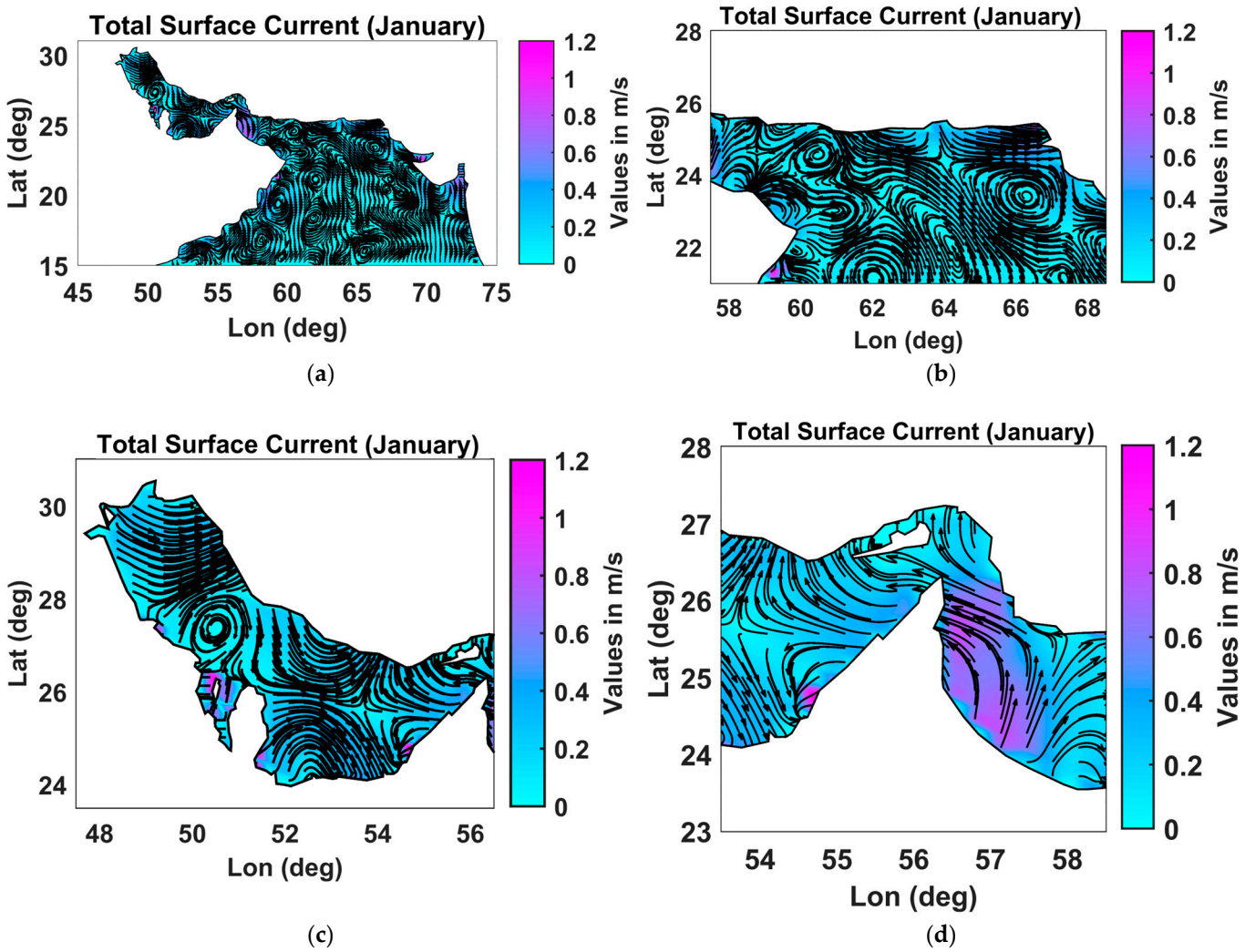

Figure 4. The TSC in January, (**a**)—the entire study area, (**b**)—the Oman Sea (region 1), (**c**)—the Persian Gulf (region 2), and (**d**)—the Strait of Hormuz (region 3).

Table 2. Statistical characteristics of current velocity in different months between 2002 and 2022 (cm/s).

Regions	Months	Mean	Std	Min	Max
Region 1 (Oman Sea)	January	5.404	9.221	0.012	101.38
	February	7.673	8.122	0.211	101.2
	March	7.668	5.241	0.157	103.2
	April	9.531	12.34	0.397	110.15
	May	10.618	5.023	1.472	106.85
	June	9.939	6.045	0.792	101.64
	July	10.794	11.347	1.118	94.876
	August	9.931	10.087	0.172	96.29
	September	8.053	4.087	0.353	90.74
	October	7.136	6.79	0.052	96.468
	November	8.697	8.942	0.286	102.51
	December	8.273	9.234	0.406	101.66
Region 2 (Persian Gulf)	January	10.652	11.476	0.001	129.4
	February	12.405	5.098	0.511	120.45
	March	12.493	8.901	0.761	122.1
	April	12.146	7.056	0.521	123.01
	May	13.563	9.551	0.373	125.58
	June	13.567	10.97	0.503	117.35
	July	11.282	6.781	0.848	101.67
	August	10.601	8.901	0.259	87.477
	September	10.246	7.321	0.249	85.179
	October	10.76	8.903	0.193	112.4
	November	12.922	5.112	0.269	133.16
	December	14.066	6.583	0.457	134.76
Region 3 (Strait of Hormuz)	January	10.146	5.403	0.001	128.36
	February	11.251	12.231	1.531	118.71
	March	11.3	8.651	1.158	112.86
	April	10.917	9.767	0.604	111.42
	May	10.541	5.239	0.252	117.13
	June	11.106	6.743	0.313	127.52
	July	10.976	9.14	0.788	115.65
	August	11.696	10.461	0.738	106.37
	September	10.804	11.031	0.668	108.89
	October	10.115	8.901	0.07	120.43
	November	12.126	9.671	0.917	133.69
	December	11.302	6.213	0.531	135.53

Generally, the current patterns show the presence of eddies in the Persian Gulf and the Oman Sea, indicating the existence of cyclonic (counterclockwise) and anticyclonic (clockwise) currents. The current directions in the Gulf of Oman exhibit more varied patterns while still conforming to broader trends. The Gulf of Oman features a complex current system with two opposing eddies—a cyclonic circulation in the western part and an anticyclonic circulation in the eastern part. Upwelling currents are present along the Iranian coastline in the areas between these opposing currents. Furthermore, an eddy current is present within the Persian Gulf region, and these currents exit from the southern portion of the Persian Gulf, as confirmed by [31]. The inflow of TSC from the Strait of Hormuz is transported to the Persian Gulf and the coastal areas (the coasts of Iran and the Arab countries). The intensity of the currents varies across different months of the year. While the character of the currents in the Persian Gulf and the northwestern and northeastern regions of the Gulf of Oman remains relatively consistent throughout the year, their intensity varies in the southwestern and southeastern parts of the Gulf of Oman and near the northern Indian Ocean.

Additionally, the current patterns in the Oman Sea and the north of the Indian Ocean are different, and their intensity varies. Eddies are observed in various regions of the Oman

Sea, indicating the intensity of the currents entering the Persian Gulf from the Oman Sea compared to the outgoing currents from this region. Seasonal variations are also evaluated to investigate the temporal variations of the TSC further. The seasonal variations of the geostrophic currents have an amplitude between 1 and 135 cm/s. Moreover, the seasonal fluctuations in the Ekman currents range between 1 and 5 cm/s. The velocity of the TSC is weaker during the spring and summer seasons and more robust in the autumn and winter. The seasonal currents also exhibit monthly-scale eddy patterns.

In the following, the data assimilation process is carried out. This procedure is performed once by assigning a unit weight to the variance–covariance matrix of the model or background (matrix B in Equation (5)) and then using the variance–covariance matrix of the background matrix obtained from Equation (5). Moreover, as mentioned in Section 2.2.2, there is a bias between the model and the observations for various reasons. To resolve this bias, more weight is given to the observations (R) to achieve a balance, as can be observed in Figures 5 and 6, which is a typical example of the data-assimilation process of the Kangan current meter station. This is achieved by selecting the appropriate variance–covariance matrix of observations considering a unit weight for the variance–covariance matrix of the model and then using the variance–covariance matrix of the background matrix obtained from Equation (5), respectively. The appropriate variance–covariance matrix of observations is obtained through an iterative process to reduce the bias between the model and the observations. This involves finding the correct variance factor. By examining the ellipses of variability between local current meter stations and the TSC estimation before and after data assimilation, there is no discrepancy in the orientation between them. Still, the TSC estimation had a bias before data assimilation, and by applying the appropriate variance–covariance matrices after data assimilation, TSC estimation approaches the observations.

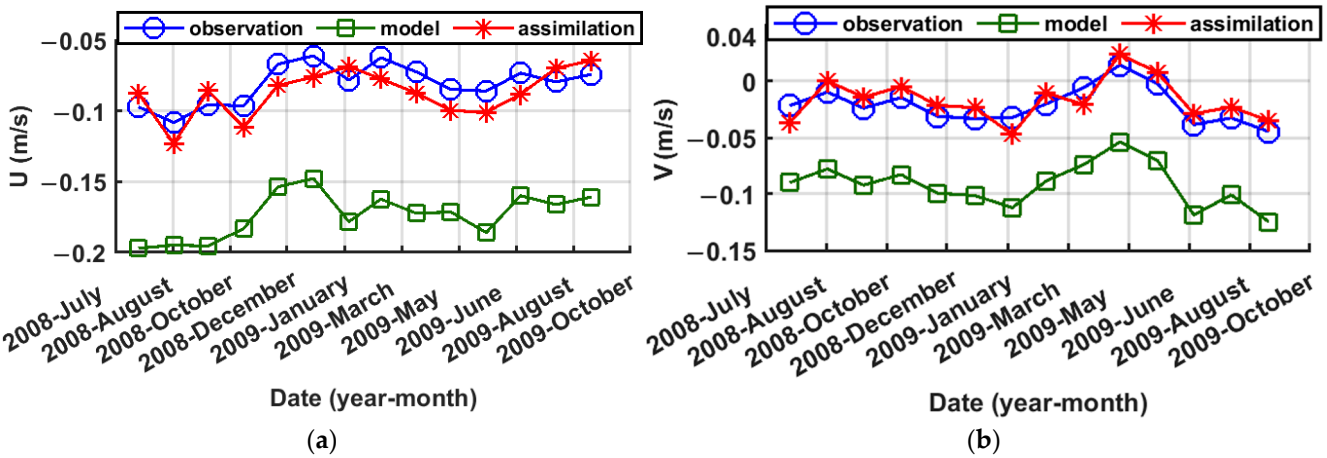

Figure 5. The data assimilation process for components of the TSC at Kangan station by selecting the appropriate variance–covariance matrix of observations and considering a unit weight for the variance–covariance matrix of the model. U (**a**) and V (**b**).

The root means square error (RMSE) between the local current meter measurements and the assimilated TSC is around 1–4 cm/s when using the matrix B, and when the identity matrix is considered, it is around 5–7 cm/s. This matter shows that the appropriate selection of matrix B may improve the accuracy of the results. Figure 7 shows the TSC components after data assimilation of the in-situ observations in January (the average of January from 2002 to 2022).

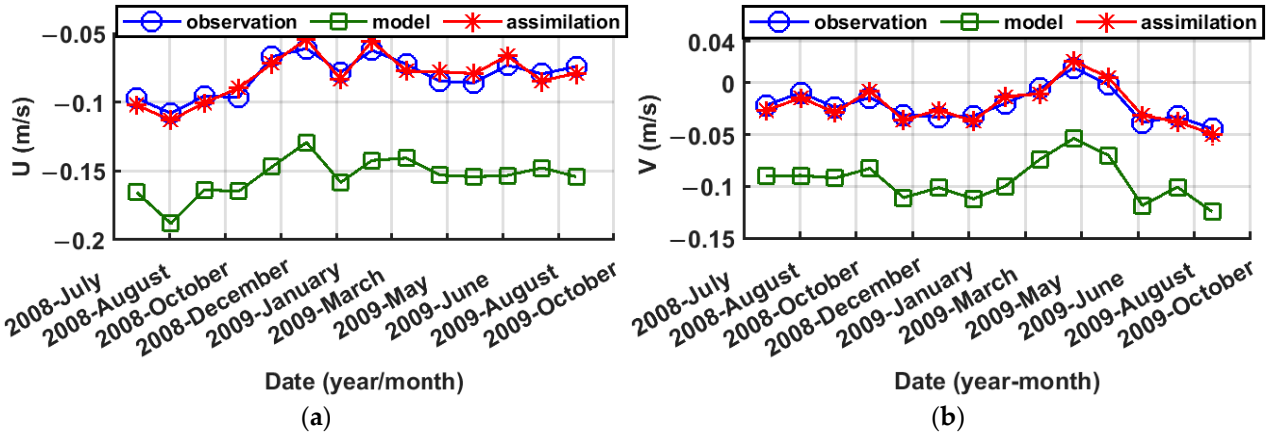

Figure 6. The data assimilation process for components of the TSC at Kangan station by selecting the appropriate variance–covariance matrix of observations and considering the variance–covariance matrix of the background matrix obtained from Equation (5). U (**a**) and V (**b**).

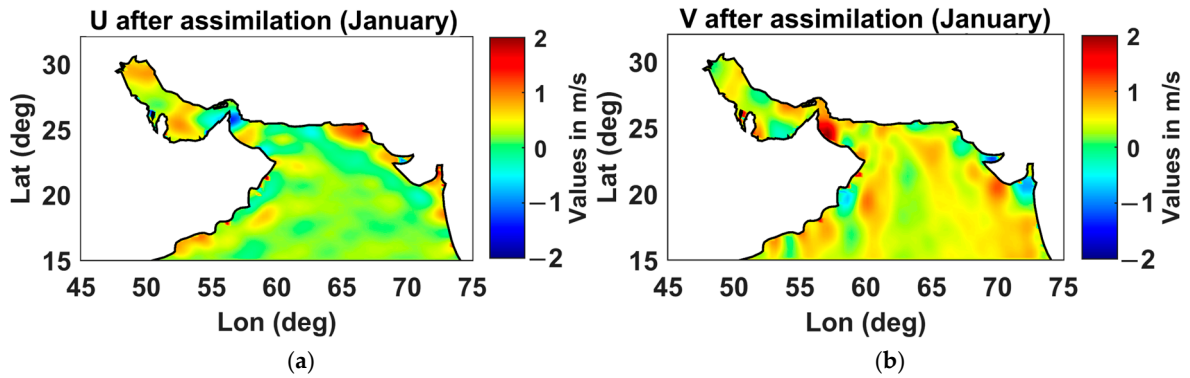

Figure 7. The components of the TSC after data assimilation (U and V) in January. U (**a**) and V (**b**).

To further investigate the benefit of data assimilation for determining the permanent surface current, the assimilated model is validated using two control stations, Nakhl Taghi and Konarak. Notably, the observations from these two stations were not involved in the data assimilation process, and therefore, they are designated as control points to examine the accuracy and performance of data assimilation. Table 3 shows the RMSE of the TSC components at these stations with and without data assimilation. As observed, data assimilation can improve the model outputs (bringing the model closer to the observations). On average, data assimilation improves the estimate of the TSC by 4 to 15 cm per second.

Additionally, to examine the advantage of data assimilation in determining the TSC, the assimilated model is validated using two control stations, Nakhl Taghi and Konarak. It is notable that the observations from these two stations were not involved in the data assimilation process, and therefore, they are designated as control points to examine the accuracy and performance of data assimilation. Table 3 shows the RMSE of the TSC components at these stations with and without data assimilation. As observed, it can enhance the model outputs (aligning the model more closely with the observations). On average, data assimilation improves the estimate of the TSC by 4 to 15 cm per second.

Table 3. The RMSE value between the TSC velocity and local current meter data at Nakhl Taghi and Konarak control stations with and without data assimilation (unit: cm/s).

Stations	Month	Before Data Assimilation	After Data Assimilation
Konarak	January	18.31	4.14
	February	10.24	5.32
	March	14.17	3.81
	April	17.22	6.11
	May	7.15	3.16
	June	9.82	5.1
	July	10.3	3.91
	August	15.68	4.21
	September	10.72	3.45
	October	12.94	4.8
	November	13.31	5.26
	December	10.74	3.44
Nakhl Taghi	January	11.26	4.21
	February	12.37	5.32
	March	11.56	4.65
	April	10.33	5.3
	May	9.62	4.12
	June	14.01	5.71
	July	12.1	4.47
	August	10.44	4.31
	September	8.11	5.53
	October	6.92	3.38
	November	7.11	6.72
	December	11.5	4.83

The CMEMS numerical model is also utilized to investigate and compare the results further. The RMSE values of the current speed in the CMEMS model at the Konarak and Nakhal Taghi control stations are 13.55 and 10.58 cm/s, respectively. In contrast, the RMSE of the current speed in the assimilated TSC is 4.69 and 4.90 cm/s (Figure 8). Figure 8 shows the comparison of the local current measurement data, the CMEMS numerical ocean model, and our approach at the Nakhal Taghi station. Overall, the average monthly RMSE from 2002 to 2022 differs by around 4 to 10 cm/s between our approach and the CMEMS model.

As you can see, the difference between the CMEMS model and the local data is that in the CMEMS model, current measurement data was not used to improve and calibrate the model in the study area. The CMEMS model lacks sufficient information to solve the boundary value problems in the study region. This issue is crucial for improving the accuracy of numerical ocean models at different regional or local scales through the available observations.

Finally, the kinetic energy in the study area is estimated by the assimilated TSC components. Figure 9 shows, as a typical example, the kinetic energy derived from the TSC for January between 2002 and 2022 in the study area according to the mentioned regional division (Oman Sea, Persian Gulf, and Strait of Hormuz). As a result, in six regions in the study area, the exploitation of the kinetic energy of the current is feasible. Figure 10 shows these six areas suitable for utilizing marine kinetic energy. Table 4 shows these six areas along with the current and kinetic energy characteristics from 2002 to 2022. The Strait of Hormuz demonstrates the most significant kinetic energy levels of the six regions examined.

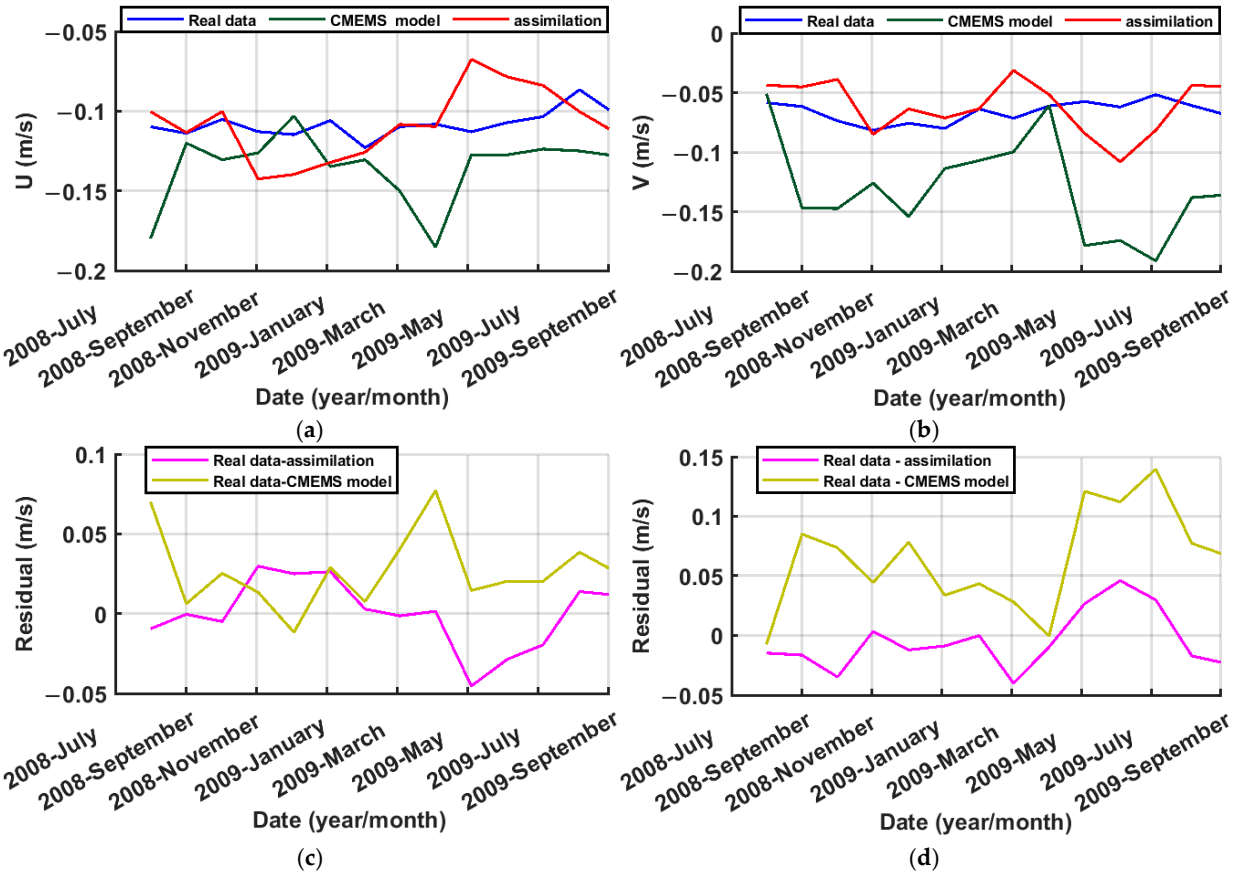

Figure 8. Comparison of the TSC components from the local station, the CMEMS model, and the assimilated TSC at the Nakhl Taghi control station. U (**a**) and V (**b**); residual of U (**c**) and residual of V (**d**).

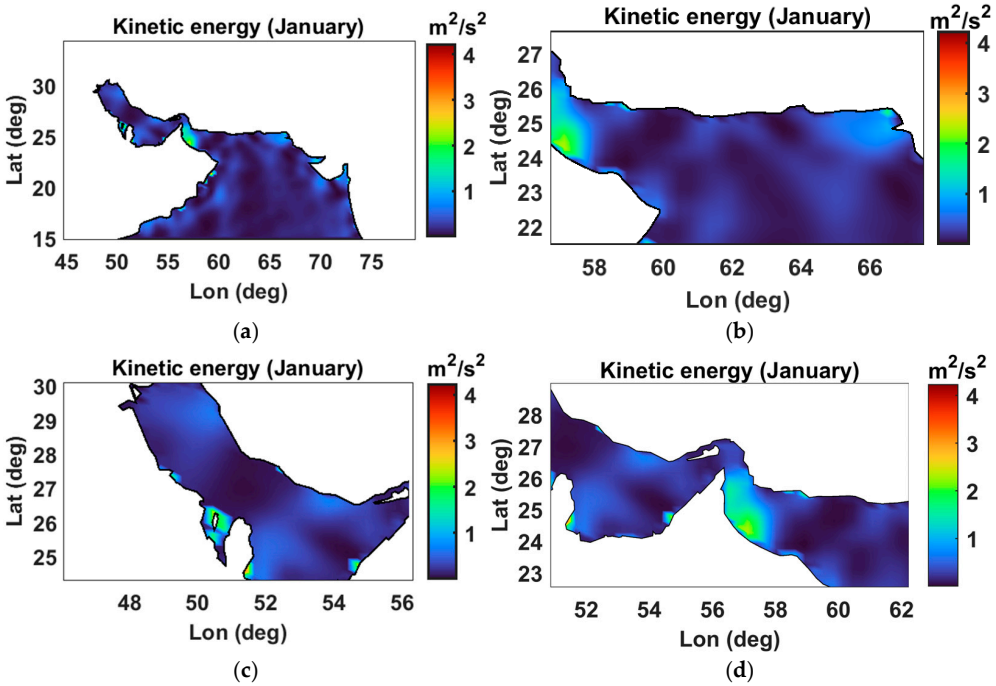

Figure 9. The kinetic energy in the region of study for January between 2002 and 2022; the entire region (**a**), the Oman Sea (**b**), the Persian Gulf (**c**), and the Strait of Hormuz (**d**).

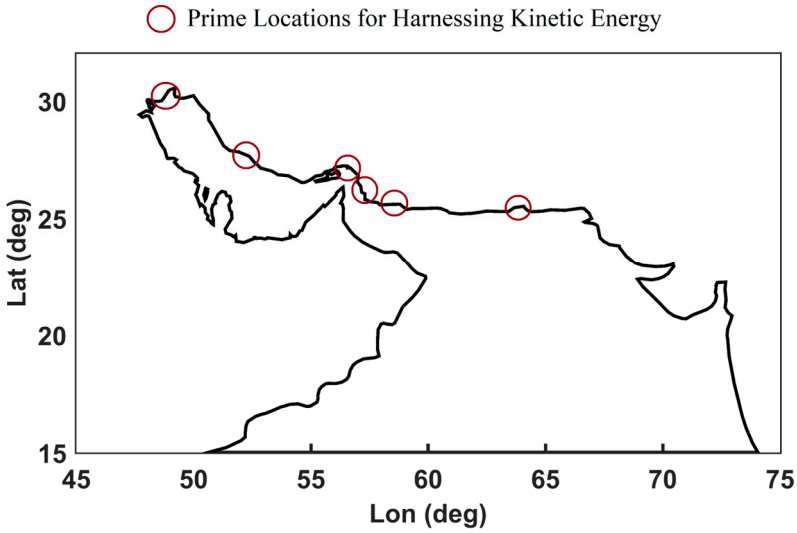

Figure 10. Areas suitable for the utilization of marine kinetic energy.

Table 4. Characteristics of the areas for the utilization of kinetic energy from the Sea.

Areas	Lat (deg)	Lon (deg)	Maximum Speed (cm/s)	Minimum Speed (cm/s)	Max Energy (m^2/s^2)	Min Energy (m^2/s^2)
khowre Musa	29.97634	49.19039	130	109	2.5	1.8
Kangan	27.61005	52.41835	119	85	2.3	1.4
Hormuz	27.02569	56.57842	135	103	2.6	1.7
Mangoli	26.14825	57.09076	130	115	2.5	1.9
Jask	25.63451	57.76305	109	91	2.1	1.5
Pasabandar	25.00698	61.35016	99	67	1.9	1.1

As mentioned in the previous sections, this study aims to determine the steady flow in the study area to assess the potential for harnessing kinetic energy. A brief review of the tidal regime is also performed in the study area. For this purpose, the analysis utilizes the TM-IR01 tidal model in the Persian Gulf and Oman Sea developed by Iran's National Cartography Center (NCC) in 2017. This model incorporates data from satellite altimetry missions and 13 coastal tide gauges, providing amplitudes and phases for 35 tidal constituents and mean sea level [33]. Tidal currents can be calculated from the amplitudes and phases of the tidal constituents using harmonic analysis, as described in [34] and the NOAA publication "Tidal Analysis and Predictions" ("https://www.tidesandcurrents.noaa.gov/publications/Tidal_Analysis_and_Predictions.pdf (accessed on 5 September 2024)"). According to this model, the tidal current velocity is around 100–140 cm/s in the Strait of Hormuz. In the Persian Gulf, the tidal current velocities tend to be lower, generally ranging from 50 to 120 cm/s. The Oman Sea also experiences tidal currents, with peak velocities around 60–110 cm/s. The results obtained are consistent and agree with previous studies' findings [32,35]. These strong tidal currents, particularly in the Strait of Hormuz, could be harnessed for tidal energy generation, providing other favorable site-specific factors. The high current velocities in the Strait of Hormuz make it one of the more promising locations for tidal energy development in this region. However, the specific site conditions, water depths, and other factors would need to be thoroughly assessed to determine the feasibility and viability of tidal energy projects in this region.

4. Discussion

This present study is a specific study aimed at proposing an approach to identify potential areas for harnessing kinetic energy from the sea using the steady-state currents obtained from geodetic data, which encompasses various issues and challenges that are

addressed. The first challenge that can be specifically mentioned is the problems with the data; due to using satellite data and global models with various limitations, the results obtained are influenced. In addition, the existing physical model is presented with extensive simplifications, which causes biases in the obtained results. The solution mentioned in this study is using data assimilation of local observations in the obtained model. Data assimilation using the 3DVar method by selecting an appropriate variance factor for the local current meter observations (matrix R) in an iterative process creates a balance, and the biases can be eliminated. It is also shown that by appropriate selection of the variance–covariance matrix of the model (matrix B), the data-assimilated model gets closer to the observations. Another challenge of this study is the effect of transient surface current, which can locally affect the current intensity. However, the goal of this study is to identify locations that are suitable for utilizing the kinetic energy from the steady-state current. Even though Ekman currents driven by wind forcing can fluctuate substantially on daily to weekly timescales, the process of averaging to a monthly timescale can help smooth out this high-frequency noise and capture a more robust representation of the general surface flow direction and magnitude. Similarly, while mesoscale eddies and other transient features certainly contribute to the flow's kinetic energy, these features are often localized in both space and time. The monthly mean currents are still able to characterize the large-scale, dominant circulation patterns that incorporate the effects of these eddies and transient phenomena, and it is suggested that in future studies, the transient component of the surface current can also be investigated. Another challenge of the present study is examining the current effect in specific local areas, which can exist in every region. In this case, the Strait of Hormuz is one of these areas that are strategically and geomorphologically important. In these specific areas, one cannot rely solely on geostrophic and Ekman currents, and for optimal site selection for sea energy extraction, other parameters such as tides, instantaneous winds, density differences, and even the shape of the coast and seabed can also be considered. Another issue realized in this study is that numerical models such as the CMEMS model need to be calibrated with local data or use local data in their boundary conditions to better respond to the current pattern. Additionally, as you know, the CMEMS model is quite straightforward. For validation, it is also possible to use other numerical models with greater capabilities that employ sigma or hybrid coordinates to better adopt to topography, such as the MIT General Circulation Model (MITGCM), the Regional Ocean Modeling System (ROMS), and the Coastal and Regional Ocean Community (CROCO), and others. Finally, another proposal that can be discussed here is the issue of investigating and modeling tidal energy as one of the most promising sources of renewable energy in the sea for harnessing kinetic energy, which includes modeling waves and tidal currents, which can be addressed.

5. Conclusions

The Persian Gulf and the Oman Sea are regions of strategic importance, not only for the global transportation of petroleum but also for the potential development of renewable energy from the sea. This study proposes a data-driven approach based on determining total surface current to identify the regions suitable for utilizing marine kinetic energy in the Persian Gulf and Oman Sea. The steady-state currents obtained from geodetic data in this region can be used to identify potential areas for harnessing kinetic energy from the sea. The persistent and strong ocean currents in the Persian Gulf and Oman Sea represent a significant renewable energy resource that could be tapped through the use of underwater turbines or other technologies. Assessing the feasibility and optimal locations for such sea energy extraction is an essential area of research. To do so, using the monthly dynamic topography gained from the geodetic data from 2002 to 2022, the geostrophic current is determined, and then by adding the Ekman current extracted from NOAA to the geostrophic current, the TSC is obtained.

Moreover, the computed TSC is improved by data assimilation of local current meter observations in the region of study through the 3DVAR techniques. The results show the

importance of selecting the appropriate covariance matrix for the model (matrix B) in the data-assimilation process. For this purpose, the RMSE between the local observations and the assimilated model velocities is in the range of 1–4 cm/s with considering B, while without considering B, it is in the range of 5–7 cm/s. Furthermore, it has been shown that the data-assimilation process for estimating the TSC with in situ data leads to a notable enhancement of 4–15 cm/s in the precision of the current estimation.

The temporal variations of the TSC behavior are investigated; the monthly TSC shows the existence of eddies in the Persian Gulf and the Oman Sea, indicating the presence of cyclonic and anticyclonic circulations. It is important to note that in the Oman Sea, the direction of the currents has varied patterns, and local currents are often observed in this region. A complex circulation with two opposing eddies is observed in the Oman Sea. Along the western side of the Oman Sea, there is a circulating eddy consistent with cyclonic motion (counterclockwise), and on the eastern side, there is an eddy with an anticyclonic motion. In the areas amid these two opposing eddies, upwelling flows arise along the Iranian shorelines.

Furthermore, the seasonal TSC shows that the current speed is lower in spring and summer, and as expected, it is higher in autumn and winter. Monthly eddies are also observed in the seasonal currents. Additionally, there is a general pattern of circulation where the surface waters of the Oman Sea move from the Strait of Hormuz towards the Persian Gulf. This movement is present throughout the year, but its speed and intensity vary across the different seasons.

Furthermore, by analyzing the kinetic energy associated with the TSC in the Persian Gulf and Oman Sea region, it is observed that the utilization of the kinetic energy within the oceanic currents and electricity generation is feasible in the study area. The assessment of the kinetic energy levels in these areas includes khowre Musa, Kangan Strait of Hormuz, Mangoli, Jask, and Pasabandar. The Strait of Hormuz has the highest kinetic energy among these six regions.

Author Contributions: Conceptualization, M.P., D.D.M. and B.V.; formal analysis, M.P., B.V., M.A.K. and A.A.; writing—original draft, M.P., B.V., M.A.K. and A.A.; supervision—review and editing, D.D.M. and B.V.; All authors have read and agreed to the published version of the manuscript.

Funding: This research is based upon research funded by the Iran National Science Foundation (INSF) under project No. 4014761.

Data Availability Statement: The datasets generated and analyzed during the current study are available from the corresponding author upon reasonable request. The data are not publicly available due to the data are part of an ongoing study.

Conflicts of Interest: The authors declare no conflicts of interest.

References

1. Tawinprai, S.; Polnumtiang, S.; Suksomprom, P.; Waewsak, J.; Tangchaichit, K. Mesoscale/Microscale Modelling for Evaluation of Wind Energy Potential and Cost Energy in Developing Country Using a High-Resolution Grid: A Case Study in the Northeastern Region of Thailand. 2023. Available online: https://assets-eu.researchsquare.com/files/rs-2828376/v1/7cd18452-d627-42ab-9e91-37b6f4c0ee1c.pdf?c=1683539992 (accessed on 5 September 2024).
2. Esteban, M.; Leary, D. Current developments and future prospects of offshore wind and ocean energy. *Appl. Energy* **2012**, *90*, 128–136. [CrossRef]
3. Torres-Herrera, H.J.; Lozano-Medina, A. Methodological Proposal for the Assessment Potential of Pumped Hydropower Energy Storage: Case of Gran Canaria Island. *Energies* **2021**, *14*, 3553. [CrossRef]
4. IPCC. Climate Change 2021: The Physical Science Basis. Contribution of Working Group I to the Sixth Assessment Report of the Intergovernmental Panel on Climate Change. 2021. Available online: https://www.ipcc.ch/report/ar6/wg1 (accessed on 5 September 2024).
5. Pujol, M.-I.; Larnicol, G. Mediterranean Sea eddy kinetic energy variability from 11 years of altimetric data. *J. Mar. Syst.* **2005**, *58*, 121–142. [CrossRef]
6. O'Rourke, F.; Boyle, F.; Reynolds, A. Tidal energy update. In *Renewable Energy*; Routledge: London, UK, 2018; pp. 451–476. [CrossRef]

7. Uihlein, A.; Magagna, D. Wave and tidal current energy—A review of the current state of research beyond technology. *Renew. Sustain. Energy Rev.* **2016**, *58*, 1070–1081. [CrossRef]
8. Coiro, D.P.; De Marco, A.; Scherillo, F.; Maisto, U.; Familio, R.; Troise, G. Harnessing marine current energy with tethered submerged systems: Experimental tests and numerical model analysis of an innovative concept. In Proceedings of the 2009 International Conference on Clean Electrical Power (ICCEP), Capri, Italy, 9–11 June 2009; pp. 76–86.
9. Mackay, E. Resource assessment for wave energy. In *Comprehensive Renewable Energy*; Elsevier: Amsterdam, The Netherlands, 2012; pp. 11–77. [CrossRef]
10. Lugo-Fernández, A.; Leben, R.R.; Hall, C.A. Kinematic metrics of the Loop Current in the Gulf of Mexico from satellite altimetry. *Dyn. Atmos. Oceans* **2016**, *76*, 268–282. [CrossRef]
11. Ruiz, S.; Pascual, A.; Garau, B.; Pujol, I.; Tintoré, J. Vertical motion in the upper ocean from glider and altimetry data. *Geophys. Res. Lett.* **2009**, *36*, L14607. [CrossRef]
12. Jiang, X.; Xie, B.; Bao, Y.; Song, Z. Global 3-hourly wind-wave and swell data for wave climate and wave energy resource research from 1950 to 2100. *Sci. Data* **2023**, *10*, 225. [CrossRef]
13. Pirooznia, M.; Voosoghi, B.; Poreh, D.; Amini, A. Integrating Hydrography Observations and Geodetic Data for Enhanced Dynamic Topography Estimation. *Remote. Sens.* **2024**, *16*, 527. [CrossRef]
14. Pirooznia, M.; Naeeni, M.R.; Tourian, M.J. Modeling total surface current in the Persian Gulf and the Oman Sea by combination of geodetic and hydrographic observations and assimilation with in situ current meter data. *Acta Geophys.* **2023**, *71*, 2839–2863. [CrossRef]
15. Pirooznia, M.; Naeeni, M.R.; Atabati, A.; Tourian, M.J. Improving the Modeling of Sea Surface Currents in the Persian Gulf and the Oman Sea Using Data Assimilation of Satellite Altimetry and Hydrographic Observations. *Remote. Sens.* **2022**, *14*, 4901. [CrossRef]
16. Chelton, D.B.; Schlax, M.G.; Samelson, R.M. Global observations of nonlinear mesoscale eddies. *Prog. Oceanogr.* **2011**, *91*, 167–216. [CrossRef]
17. Poulain, P.-M.; Gerin, R.; Mauri, E.; Pennel, R. Wind Effects on Drogued and Undrogued Drifters in the Eastern Mediterranean. *J. Atmospheric Ocean. Technol.* **2009**, *26*, 1144–1156. [CrossRef]
18. Stammer, D.; Wunsch, C. Preliminary assessment of the accuracy and precision of TOPEX/POSEIDON altimeter data with respect to the large-scale ocean circulation. *J. Geophys. Res. Oceans* **1994**, *99*, 24584–24604. [CrossRef]
19. Rio, M.-H.; Poulain, P.-M.; Pascual, A.; Mauri, E.; Larnicol, G.; Santoleri, R. A Mean Dynamic Topography of the Mediterranean Sea computed from altimetric data, in-situ measurements and a general circulation model. *J. Mar. Syst.* **2007**, *65*, 484–508. [CrossRef]
20. Escudier, R.; Bouffard, J.; Pascual, A.; Poulain, P.; Pujol, M. Improvement of coastal and mesoscale observation from space: Application to the northwestern Mediterranean Sea. *Geophys. Res. Lett.* **2013**, *40*, 2148–2153. [CrossRef]
21. Sudre, J.; Maes, C.; Garçon, V. On the global estimates of geostrophic and Ekman surface currents. *Limnol. Oceanogr. Fluids Environ.* **2013**, *3*, 1–20. [CrossRef]
22. Raj, R.P. Surface velocity estimates of the north Indian Ocean from satellite gravity and altimeter missions. *Int. J. Remote Sens.* **2016**, *38*, 296–313. [CrossRef]
23. Poulain, P.; Menna, M.; Mauri, E. Surface geostrophic circulation of the Mediterranean Sea derived from drifter and satellite altimeter data. *J. Phys. Oceanogr.* **2012**, *42*, 973–990. [CrossRef]
24. Carrillo, L.; Palacios-Hernández, E. Seasonal evolution of the geostrophic circulation in the northern Gulf of California. *Estuar. Coast. Shelf Sci.* **2002**, *54*, 157–173. [CrossRef]
25. Palma-Lara, D.; Carrillo, L.; Trasviña-Castro, A.; Reyes-Mendoza, O.; Valle-Rodríguez, J. Analysis of coastal altimetry in the Mexican Caribbean. *Adv. Space Res.* **2023**, *71*, 964–974. [CrossRef]
26. Sellers, C.; Ammirati, L.; Khalili, M.A.; Buján, S.; Rodas, R.A.; Di Martire, D. The Use DInSAR Technique for the Study of Land Subsidence Associated with Illegal Mining Activities in Zaruma–Ecuador, a Cultural Heritage Cite. In *European Workshop on Structural Health Monitoring*; Rizzo, P., Milazzo, A., Eds.; EWSHM Lecture Notes in Civil Engineering; Springer: Cham, Switzerland, 2023. [CrossRef]
27. Khalili, M.A.; Guerriero, L.; Pouralizadeh, M.; Calcaterra, D.; Di Martire, D. Prediction of Deformation Caused by Landslides Based on Graph Convolution Networks Algorithm and Dinsar Technique. *ISPRS Ann. Photogramm. Remote. Sens. Spat. Inf. Sci.* **2023**, *X-4/W1-202*, 391–397. [CrossRef]
28. Ide, K.; Courtier, P.; Ghil, M.; Lorenc, A.C. Unified Notation for Data Assimilation: Operational, Sequential and Variational (gtSpecial IssueItData Assimilation in Meteology and Oceanography: Theory and Practice). *J. Meteorol. Soc. Jpn. Ser. II* **1997**, *75*, 181–189. [CrossRef]
29. Cushman-Roisin, B.; Beckers, J.M. Chapter 7—Geostrophic Flows and Vorticity Dynamics. In *Introduction to Geophysical Fluid Dynamics: Physical and Numerical Aspects*; Academic Press: Cambridge, MA, USA, 2011; Volume 101, pp. 205–238.
30. Shenoi, S.S.; Saji, P.K.; Almeida, A.M. Near-surface circulation and kinetic energy in the tropical Indian Ocean de-rived from lagrangian drifters. *J. Mar. Res.* **1999**, *57*, 885–907. [CrossRef]
31. Reynolds, R.M. Physical oceanography of the Gulf, Strait of Hormuz, and the Gulf of Oman—Results from the Mt Mitchell expedition. *Mar. Pollut. Bull.* **1993**, *27*, 35–59. [CrossRef]

32. Fallahi, M.; Torabi Azad, M.; Mansoury, D. A Hydrodynamic Model of Tidal Current in the Strait of Hormuz. *Int. J. Coast. Offshore Environ. Eng.* **2021**, *6*, 37–45. [CrossRef]
33. Soltanpour, A.; Pirooznia, M.; Aminjafari, S.; Zareian, P. Persian Gulf and Oman Sea tide modeling using satellite altimetry and tide gauge data (TM-IR01). *Mar. Georesources Geotechnol.* **2017**, *36*, 677–687. [CrossRef]
34. Pugh, D.T. *Tides, Surges and Mean Sea-Level*; John Wiley & Sons: Chichester, UK, 1987.
35. Pous, S.P.; Carton, X.; Lazure, P. Hydrology and circulation in the Strait of Hormuz and the Gulf of Oman—Results from the GOGP99 Experiment: Strait of Hormuz. *J. Geophys. Res. Oceans* **2004**, *109*, C12037. [CrossRef]